

# Increased fluctuation in the edge tokamak plasmas with the resonant magnetic perturbation field

Minjun J. Choi,<sup>1, a)</sup> Jae-Min Kwon,<sup>1</sup> Juhyung Kim,<sup>1</sup> Tongnyeol Rhee,<sup>1</sup> Jun-Gyo Bak,<sup>1</sup> Giwook Shin,<sup>1</sup> Hyun-Seok Kim,<sup>1</sup> Byoung-Ho Park,<sup>1</sup> Hogun Jhang,<sup>1</sup> Gunsu S. Yun,<sup>2</sup> Minwoo Kim,<sup>1</sup> Jong-Kyu Park,<sup>3</sup> SangKyeun Kim,<sup>3</sup> Hyung Ho Lee,<sup>1</sup> Yongkyoon In,<sup>4</sup> Kimin Kim,<sup>1</sup> Jaehyun Lee,<sup>1</sup> Min Ho Kim,<sup>2</sup> and Hyeon K. Park<sup>4</sup>

<sup>1)</sup>*Korea Institute of Fusion Energy, Daejeon 34133, Republic of Korea*

<sup>2)</sup>*Pohang University of Science and Technology, Pohang, Gyungbuk 37673, Republic of Korea*

<sup>3)</sup>*Princeton Plasma Physics Laboratory, Princeton, New Jersey 08543, USA*

<sup>4)</sup>*Ulsan National Institute of Science and Technology, Ulsan 44919, Republic of Korea*

(Dated: 23 December 2024)

The resonant magnetic perturbation (RMP) field has been utilized to suppress the edge localized mode (ELM) in tokamak plasmas. The pedestal top during the RMP ELM suppression is characterized by the increased broadband fluctuation, i.e. plasma turbulence. The origin of the increased fluctuation and its characteristics were not fully understood. Here, we show that the increased fluctuation involves the weak but significant nonlinear coupling in a narrow region at the pedestal top and the spatial structure of turbulence becomes less predictable around that region as expected for the stochastic fields around magnetic islands. We analyzed the bicoherence and the rescaled Jensen-Shannon complexity of the electron temperature fluctuation measured in KSTAR experiment to identify the nonlinear coupling and the change of statistical turbulence characteristics, respectively. Our analyses suggest that the nonlinear coupling through a partially stochastic island layer at the pedestal top contributes to the fluctuation increase during the RMP ELM suppression.

arXiv:2102.10733v5 [physics.plasm-ph] 26 Oct 2021

---

<sup>a)</sup>[mjchoi@kfe.re.kr](mailto:mjchoi@kfe.re.kr)

## INTRODUCTION

The edge localized mode (ELM) is a peeling-ballooning instability driven by the large current density and the steep pressure gradient in the high confinement mode (H-mode) pedestal in tokamak plasmas. Periodic collapses of the pedestal due to the explosive growth of the ELM have been a serious issue for steady-state operation of the H-mode plasmas. Applying the resonant magnetic perturbation (RMP) field is the most developed method to suppress the ELM and its pedestal collapse<sup>1-6</sup>. Since the first demonstration of the RMP ELM suppression<sup>1</sup>, many researches have followed for in-depth understanding of its mechanism. The initial idea of the stochastic edge transport<sup>7</sup> was suggested<sup>1</sup>, and later a narrow and localized stochastic layer was considered promising to explain the experimental edge transport<sup>8</sup> and the ELM stability<sup>9</sup> with the RMP field. Resonant penetration of the perturbation field and consequent temperature flattening near the pedestal top were observed in the RMP ELM suppression experiment<sup>10</sup>, supporting the narrow stochastic layer formation inside the plasma<sup>11</sup>. In addition, the recent two-fluid MHD simulation could reproduce the entire ELM control process through the sequential formation of narrow and separated stochastic layers at the pedestal foot and top<sup>12</sup>.

One prominent characteristics of the RMP ELM suppressed pedestal is the increase of broadband fluctuation, i.e. plasma turbulence<sup>13-15</sup>. In particular, the KSTAR experiment shows that the fluctuation is locally enhanced near the pedestal top<sup>14</sup>. Despite the importance of turbulence in the pedestal transport, the origin of the increased fluctuation and its characteristics were not fully understood. The nonlinear coupling between a remnant edge localized mode and turbulence was suggested to explain the increased fluctuation in some KSTAR experiment<sup>14</sup>, and it was attributed to the change of pressure gradients<sup>15</sup> or flow shear<sup>16,17</sup> in other researches. A link between the stochastic layer and turbulence behavior remains unclear, though the stochastic layer has been considered crucial to explain many aspects of the RMP ELM suppression experiment.

It is worth reminding that there have been reports of the nonlinear coupling between magnetic islands and turbulence<sup>18-22</sup> which can lead to turbulence enhancement. Motivated by previous researches, we suggest that a layer of the partially stochastic island contributes to the increased fluctuation through the nonlinear coupling in the RMP ELM suppressed pedestal. We used the wavelet bicoherence analysis<sup>23</sup> to obtain the fast temporal evolution of the nonlinear coupling strength in the pedestal electron temperature fluctuation measured by the electron cyclotron emission imaging (ECEI) diagnostics<sup>24</sup> of KSTAR<sup>25</sup>. Instantaneous and synchronized increase of the temperature fluctuation amplitude and the bicoherence is observed at the pedestal top with an abrupt transition to the ELM suppression from the mitigation. To find support for the field penetration at the pedestal top when the fluctuation amplitude and bicoherence increase, the analysis of the Jensen

Shannon complexity and the normalized Shannon entropy<sup>26</sup> is used to investigate the statistical characteristics of the pedestal turbulence structure recorded in the temperature fluctuation. The stochastic fields around a magnetic island are expected to affect turbulence and make its structure different from those grown over the unperturbed pedestal<sup>27,28</sup>. The increased fluctuation in the RMP ELM suppressed pedestal yields a less predictable state compared to the ELMing or the ELM mitigated pedestal state. It is also in contrast to that the increased fluctuation in the natural ELM free pedestal develops a distinguishable structure. This analysis could be used to estimate the layer width over which the fluctuation is statistically less predictable, and evolution of this width is found to be correlated with the RMP field application and the electron heat transport change. Our analyses show that the increased fluctuation with the RMP ELM suppression involves the nonlinear coupling at the pedestal top where its statistical characteristics implies the existence of a partially stochastic island layer.

## EXPERIMENT AND ANALYSIS

An example of the RMP ELM suppression in the KSTAR H-mode deuterium plasma #18945 is shown in Fig. 1. The  $n = 1$  RMP field is applied from  $t = 3.5$  sec and its strength increases in time as shown in Fig. 1(a). Fig. 1(b) shows that the line averaged plasma density ( $n_e$ ) drops about 17 % with applying the RMP field while the edge electron temperature ( $T_e$ ) drops about 9 %, i.e. the so-called density pump-out.  $n_e$  and  $T_e$  are obtained by two color interferometry diagnostics<sup>29</sup> and the electron cyclotron emission diagnostics<sup>30</sup>, respectively. The ELM crash is mitigated with the RMP field and it is completely suppressed after  $t \sim 6.2$  sec as shown by the divertor  $D_{\alpha}$  emission signal<sup>31</sup> whose sharp rise indicates the ELM crash event. Modest decrease of  $n_e$  and the edge  $T_e$  during an abrupt transition from the ELM mitigation to the ELM suppression is observed, indicating that the pedestal pressure height is reduced to make the ELM stable.

The  $T_e$  fluctuation at the pedestal top ( $R_{\text{ped}}$ ) increases with the abrupt transition to the ELM suppression and remains at a higher level during the suppression phase as shown in Fig. 1(c). Local measurement of the  $T_e$  fluctuation is provided by the electron cyclotron emission imaging (ECEI) diagnostics<sup>24,32,33</sup>, and the pedestal top location is identified by the strongest ELM precursor location. Since the penetration of the RMP field near the pedestal top has been considered as a key mechanism of the RMP ELM suppression<sup>8-12</sup>, it would not be strange to hypothesize that the increased fluctuation is associated with magnetic islands or stochastic fields resulting from the field penetration at the pedestal top. It is possible that the pressure profile variation by the transport change with the perturbed magnetic geometry results in a stronger linear drive for ambient turbulence. In this paper, we consider a different contribution through the nonlinear

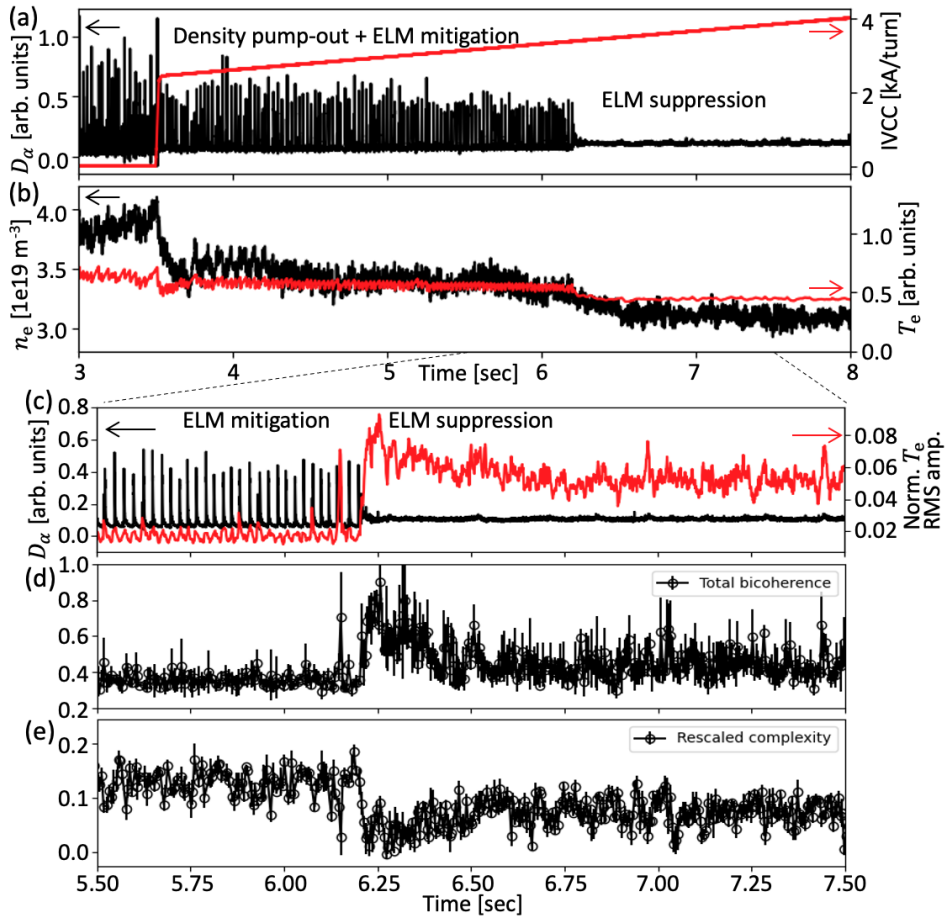


FIG. 1. (Color online) (a) The  $D_{\alpha}$  emission (black) and the in-vessel coil current for the resonant magnetic perturbation (RMP) field (red). The edge localized mode (ELM) is suppressed with the increasing RMP field. (b) The line averaged plasma density ( $n_e$ ) and the pedestal electron temperature ( $T_e$ ). (c) Expanded view of the  $D_{\alpha}$  emission (black) and the normalized  $T_e$  fluctuation root-mean-square amplitude (red). (d) The total summed bicoherence and (e) the rescaled Jensen Shannon complexity of the  $T_e$  fluctuation at the pedestal top. Error bars indicate the standard deviation of the measurement.

coupling between magnetic islands with the stochastic fields and ambient turbulence for turbulence enhancement.

We firstly analyzed the bicoherence in the temperature fluctuation to identify the nonlinear coupling. The bicoherence is a well known method to detect the strength of the phase coupling among three fluctuations<sup>34</sup>. For the fast temporal resolution of the bicoherence calculation during the abrupt ELM suppression transition, the Morlet wavelet transformation<sup>23</sup> is utilized instead of the conventional Fourier transformation<sup>34</sup>. The evolution of total summed bicoherence ( $< 100$  kHz) in the temperature fluctuation measured at the pedestal top is plotted in Fig. 1(d). The bicoherence sharply increases in sync with the abrupt ELM suppression transition (the field penetration) and its level remains a little but significantly higher than the level during the ELM mitigation or before the

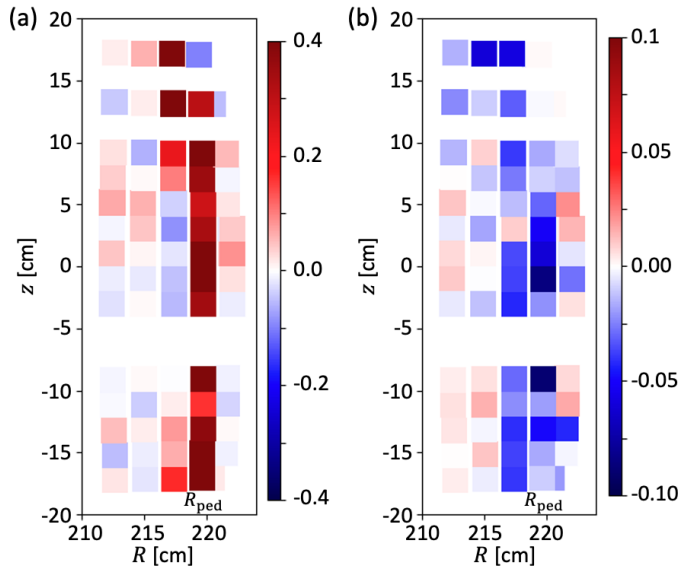


FIG. 2. (Color online) Two-dimensional measurement of (a) the bicoherence and (b) the rescaled complexity change between the ELM mitigation and suppression phases.

RMP field application. This behavior is similar with the fluctuation amplitude evolution shown in Fig. 1(c). The bicoherence increase is dominated by multiple distinguished three-wave interactions including a low frequency  $< 5$  kHz components. Two-dimensional measurement of the bicoherence change between the ELM mitigation and suppression phases in Fig. 2(a) shows that the bicoherence increment is localized at the pedestal top. Note that some channels whose noise contributions are exceptional and the data during the ELM crash period are excluded in all the analysis.

The correlation between the bicoherence and fluctuation amplitude implies the role of the nonlinear coupling in the fluctuation increase, although measurement uncertainties in the pedestal profiles (linear drive) hinder accurate quantitative analysis. Temporal synchronization and spatial locality of the bicoherence increase with respect to the ELM suppression transition timing and  $R_{\text{ped}}$  imply involvement of magnetic islands or stochastic fields. In fact, previous researches showed that the nonlinear coupling through a magnetic island<sup>18-21</sup> can occur and result in turbulence enhancement. Evidence for magnetic islands or stochastic fields in the experiment would be helpful for corroboration.

Although a direct measurement of fine structures of the magnetic field is not possible in high temperature pedestals, local measurement of other plasma parameters can be utilized to investigate the pedestal structure and find support for the field line stochasticization. Turbulence structure over the stochastic fields around magnetic islands are expected to have a different structure from that grown over the unperturbed pedestal, e.g. turbulence structure can lock on to the structure of stochastic fields<sup>28</sup>. We used a statistical method known as the complexity and entropy analysis<sup>26</sup> to distinguish turbulence structure recorded in the temperature fluctuation. This analysis tells whether

the fluctuation has a few dominant patterns or close to the less predictive fluctuation with more distributed patterns. Here, a pattern means an order in the amplitude. For example, the first segment of size  $d = 3$  of a serial data  $x = \{x_i\}_{i=1,\dots,N} = \{4, 7, 9, 6, \dots, x_N\}$  is  $\{4, 7, 9\}$ , and the order of its elements is simply increasing and can be represented by  $(1, 2, 3)$ . The second segment is  $\{7, 9, 6\}$  and the order is  $(3, 1, 2)$ . The probability distribution of orders of segment elements is known as the Bandt-Pompe (BP) probability distribution function<sup>35</sup>. Note that  $N$  should be large enough than  $d!$  ( $N \gg d!$ ) for the reliable calculation of the BP probability. Using the BP probability of a given data, the Jensen Shannon complexity ( $C_{\text{JS}}$ ) and the normalized Shannon entropy ( $H$ ) can be calculated. The Jensen Shannon complexity ( $C_{\text{JS}} = QH$ ) is defined as the product of the normalized Shannon entropy  $H = S/S_{\text{max}}$ , where  $S = S(P) = -\sum_i p_i \log(p_i)$  is the Shannon entropy of the given probability distribution function  $P = \{p_i\}$  and  $S_{\text{max}}$  is the maximum entropy, and the Jensen Shannon divergence  $Q \propto S\left(\frac{P+P_e}{2}\right) - \frac{S(P)}{2} - \frac{S(P_e)}{2}$  where  $P_e$  is the uniform probability distribution function. It measures kind of the distance between the given probability distribution function and the uniform probability distribution function. The comparison of a given data against the fractional Brownian motion or fractional Gaussian noise data on the  $C_{\text{JS}}-H$  plane is shown as a useful method to distinguish the fluctuation with a dominant patterns (chaotic signal) from less predictable fluctuation (stochastic signal)<sup>26</sup>. For the efficient comparison,  $C_{\text{JS}}$  is rescaled as

$$\hat{C} = \frac{C_{\text{JS}} - C_0}{|C_{\text{bdry}} - C_0|} \quad (1)$$

where  $C_0(H)$  is the Jensen Shannon complexity of fBm or fGn signals and  $C_{\text{bdry}}(H)$  is the maximum (if  $C_{\text{JS}} > C_0$ ) or minimum (if  $C_{\text{JS}} < C_0$ ) Jensen Shannon complexity at the given  $H$ <sup>36,37</sup>. The rescaled complexity ( $\hat{C}$ ) ranges from -1 ( $C_{\text{JS}} = C_{\text{min}}$ ) to 1 ( $C_{\text{JS}} = C_{\text{max}}$ ), and the less  $\hat{C}$  means the less predictable.

The analysis result on the temperature fluctuation at  $R_{\text{ped}}$  shows that the rescaled Jensen Shannon complexity ( $\hat{C}$ ) decreases with the ELM suppression transition and remains lower for the suppression phase than that of other phases as shown in Fig. 1(e). In the analysis, the BP probability calculation parameters such as  $d$  and  $N$  were set to  $d = 5$  and  $N = 2500$  to satisfy  $N \gg d! = 120$  and  $d\Delta t$  where  $\Delta t = 2$  us is a time step of the temperature fluctuation data can be order of the transit time of pedestal turbulence structures over the measurement channel area. The reduced  $\hat{C}$  means that the pedestal structure recorded in the temperature fluctuation becomes less predictable in the ELM suppression phase. Two-dimensional measurement of the  $\hat{C}$  change between the ELM mitigation and suppression phases is shown in Fig. 2(b). It shows that  $\hat{C}$  decreases in some radial region localized at  $R_{\text{ped}}$ .

Compared to the region of the bicoherence increase shown in Fig. 2(a), the  $\hat{C}$  reduction region

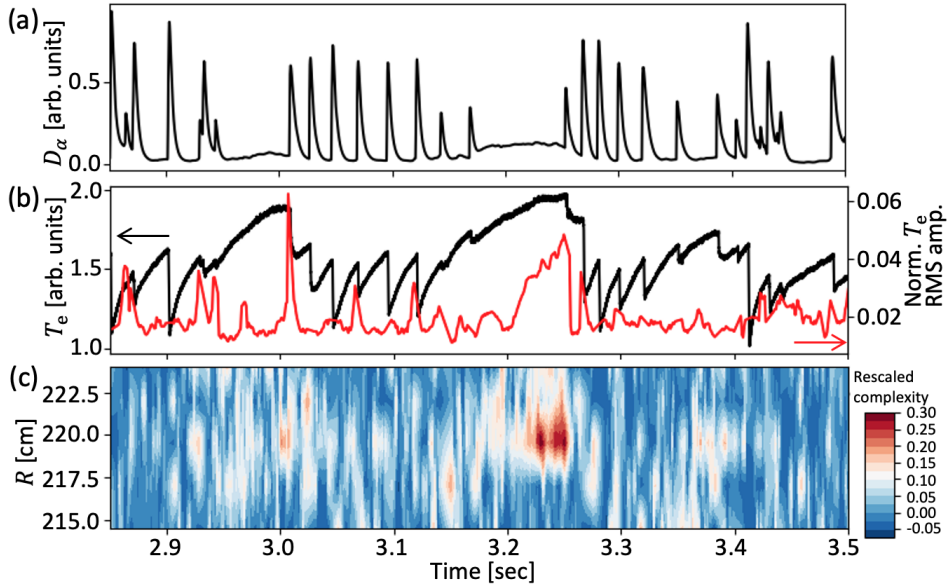


FIG. 3. (Color online) (a) The  $D_{\alpha}$  emission and (b) electron temperature ( $T_e$ ) (black) and the normalized  $T_e$  fluctuation root-mean-square amplitude at the pedestal top (red). (c) Spatiotemporal evolution of the rescaled Jensen Shannon complexity of  $T_e$  fluctuation around the pedestal top.

is a little broader especially around the midplane. This indicates that one analysis is not directly related to the other, though they can have the common origin, e.g. a layer of the partially stochastic island at  $R_{\text{ped}}$ . Our interpretation is that the nonlinear coupling with a partially stochastic magnetic island is more localized at  $R_{\text{ped}}$  and the stochastic fields around the island affect turbulence structure around  $R_{\text{ped}}$ .

One may consider that the reduced  $\hat{C}$ , i.e. less predictable distribution of temperature fluctuation patterns, is simply due to the increased broadband fluctuation instead of the field line stochasticization. Fig. 3 shows the analysis of  $\hat{C}$  in the H-mode plasma including a natural ELM free phase without the external perturbation field. The natural ELM free phase appears around 3.25 sec. The pedestal grows without the ELM crash and the broadband temperature fluctuation amplitude increases significantly as shown in Fig. 3(b). The spectral analysis found that the increased fluctuation in both the RMP ELM suppression phase and the natural ELM free phase has the similar wavenumber distribution ( $k_{\theta}\rho_i < 1$  where  $k_{\theta}$  is the poloidal wavenumber and  $\rho_i$  is the ion Larmor radius). Spatiotemporal evolution of  $\hat{C}$  of the temperature fluctuation near  $R_{\text{ped}}$  is shown in Fig. 3(c). In contrast to the RMP ELM suppression case,  $\hat{C}$  increases during the natural ELM free phase with the increased fluctuation. It means that turbulence develops to have a more distinguishable structure (regular pattern) in the natural ELM free phase without the perturbation field, while it couldn't in the RMP ELM suppression phase possibly due to locking on to the stochastic fields<sup>28</sup>.

Another result supporting that the  $\hat{C}$  reduction reflects the field penetration effect could be temporal evolution of the  $\hat{C}$  reduction width. To estimate the width of the reduced  $\hat{C}$  region,  $\hat{C}$  measurements using the ECEI channels over two-dimensional  $(R, z)$  space are projected on the radial axis including the plasma vertical center based on the equilibrium reconstruction using EFIT<sup>38</sup>. The time averaged profiles of the  $\hat{C}$  along the radial axis are shown in Fig. 4(a). Since each channel has different noise contribution, the relative change of profiles between different averaging periods is more meaningful than their absolute values. The averaged  $\hat{C}$  profile is nearly same between the H-mode phase w/o the RMP (black crosses) and the ELM mitigation phase w/ the RMP (blue circles). A significant drop compared to values of other periods is observed near  $R_{\text{ped}}$  in the initial ELM suppression period w/ the RMP (red squares). The full width of the reduced  $\hat{C}$  region can be estimated as the range of the  $\hat{C}$  reduction more than the standard deviation of  $\hat{C}$  measurements, which is about  $2.6 \pm 2.0$  cm considering the finite size ( $\sim 2$  cm) of measurement area of each channel. The flux surface distortion by the plasma kink response which caused the overestimation should be taken into account for a more accurate estimation. Fig. 4(b) shows evolution of the  $\hat{C}$  reduction width in the plasma #18945 introduced in Fig. 1. When the RMP field is applied around 3.5 sec and the electron temperature drops transiently, the  $\hat{C}$  reduction over a significant region is captured for this transient moment. It decreases back to the zero level when the plasma enters to the mitigated ELMing phase with the partially recovered pedestal with the field screening. The pedestal temperature level decreases slowly with the increasing RMP field strength. The  $\hat{C}$  reduction width increases to a significant level with a transition to the ELM suppression phase of the enhanced electron heat transport. Although it is not shown in this paper, the similar correlation of the  $\hat{C}$  reduction with the RMP field strength increase and the electron heat transport enhancement was observed in the adaptive RMP control experiment<sup>39</sup>. These observations support that the  $\hat{C}$  reduction reflects the field penetration at the pedestal top which is responsible for the electron heat transport enhancement or the ELM suppression.

It would be interesting to compare the observed  $\hat{C}$  evolution with the result of the recent two-fluid numerical simulation<sup>12</sup> using TM1 code<sup>40</sup> based on DIII-D plasma equilibrium<sup>41</sup>. Firstly, the simulation suggested that the sequential formation of the stochastic layers at the pedestal foot and top could explain the density pump-out in the ELM mitigation phase and the ELM suppression, respectively. The reduced  $\hat{C}$  of the pedestal top temperature fluctuation in the ELM suppression phase is not inconsistent with the simulation result, but no evidence for multiple separated layers (reduced  $\hat{C}$  regions) is found. However, the ECE measurement in the pedestal foot region is uncertain due to the limited diagnostics capability with the low density and temperature of that region. Although a reliable analysis based on local ECE measurement was not available in the pedestal foot

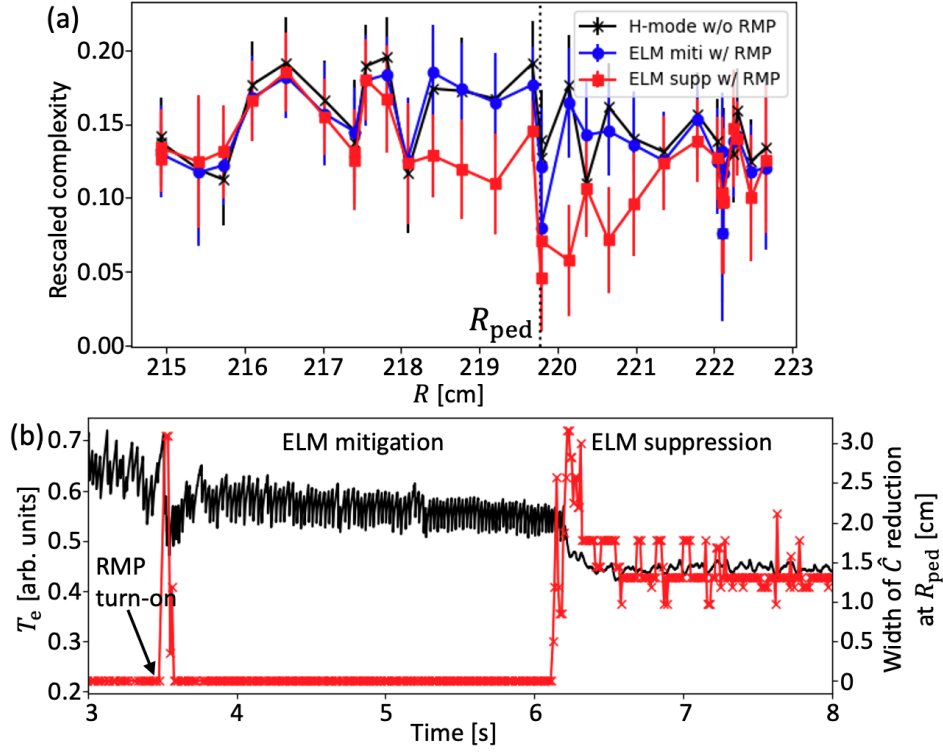


FIG. 4. (Color online) (a) Radial profiles of the time averaged rescaled complexity ( $\hat{C}$ ) of electron temperature fluctuation in different phases. The pedestal top ( $R_{\text{ped}}$ ) is indicated by black dashed line. Error bars indicate the standard deviation during the time average period. (b) The pedestal electron temperature ( $T_e$ ) (black) and the width of reduced  $\hat{C}$  region (red) in time.

region, the measurements using a Langmuir probe<sup>42</sup> could be used to investigate the fluctuation and transport behavior in the far edge region<sup>43</sup>. Analyses on the particle flux measured by the divertor Langmuir probe showed that  $\hat{C}$  of the particle flux near the striking point reduces more and more as the plasma state changes from the H-mode to the ELM mitigation and from the ELM mitigation to the ELM suppression. This sequential  $\hat{C}$  reduction of the particle flux can be associated with the increasing RMP field response in the edge region from the H-mode ELMing phase to the RMP ELM suppression phase. However, the divertor measurements can be affected by other scrape-off layer physics, and they might not reflect the internal plasma state correctly. The kinetic simulation and analyses of internal measurements using the reciprocating Langmuir probe are left for future work to demonstrate the sequential plasma response observed in the TM1 simulation. Secondly, for the quantitative comparison of the stochastic layer width at the pedestal top, a sophisticated cross validation research matching all the important parameters such as the plasma resistivity would be necessary. Also, more efforts are required to resolve the measurement uncertainty originated from the equilibrium and profile uncertainties. Thirdly, although the TM1 simulation has shown a good agreement with the DIII-D experiment on the RMP applied edge transport without considering

evolution of turbulence transport, our analyses suggest that turbulence can be affected by magnetic islands and stochastic fields. The regime where the TM1 showed the good agreement may correspond to a regime where turbulence transport is less significant to other transport process.

## SUMMARY

In summary, we analyzed electron temperature fluctuation to understand the origin of the increased fluctuation level in the RMP ELM suppression experiment. We suggest that the localized nonlinear coupling through a partially stochastic island layer contributes to the fluctuation increase, which can be incorporated with the RMP field penetration phenomena during the ELM suppression. The bicoherence and rescaled complexity analyses are used to investigate the nonlinear coupling strength and the pattern distribution of the fluctuation. The analysis results are not inconsistent with the expected consequences of a partially stochastic island layer. In particular, the latter analysis can be used to distinguish a pedestal turbulence state under the RMP field, which would help to understand different RMP ELM suppression mechanisms. Although identification of a specific mechanism of the nonlinear coupling is beyond the scope of this work, it would be interesting to note that the nonlinear resonance condition described in reference<sup>18</sup> can be satisfied in the RMP ELM suppression experiment, i.e. the island width which is expected to be around the half of the stochastic layer (the reduced  $\hat{C}$  region) is about a multiple of the ion Larmor radius and the island frequency ( $\omega$ ) condition can be also satisfied as  $\omega_E \approx \omega < \omega_{*e}$  where  $\omega_E$  is the electric drift frequency and  $\omega_{*e}$  is the electron diamagnetic drift frequency.

## ACKNOWLEDGMENTS

The authors would like to express sincere gratitude to the KSTAR team. M.J.C. acknowledges helpful discussion with M. Cao and P.H. Diamond during the 6th Asia-Pacific Transport Working Group meeting. This research was supported by R&D Programs of “KSTAR Experimental Collaboration and Fusion Plasma Research(EN2101-12)” and “High Performance Fusion Simulation R&D(EN2141-7)” through Korea Institute of Fusion Energy (KFE) funded by the Government funds and by National Research Foundation of Korea under NRF-2019M1A7A1A03088462.

## REFERENCES

- <sup>1</sup>T. E. Evans, R. A. Moyer, P. R. Thomas, J. G. Watkins, T. H. Osborne, J. a. Boedo, E. J. Doyle, M. E. Fenstermacher, K. H. Finken, R. J. Groebner, M. Groth, J. H. Harris, R. J. La Haye, C. J.

- Lasnier, S. Masuzaki, N. Ohyabu, D. G. Pretty, T. L. Rhodes, H. Reimerdes, D. L. Rudakov, M. J. Schaffer, G. Wang, and L. Zeng, *Physical Review Letters* **92**, 235003 (2004).
- <sup>2</sup>Y. Liang, H. Koslowski, P. Thomas, E. Nardon, B. Alper, P. Andrew, Y. Andrew, G. Arnoux, Y. Baranov, M. Becoulet, M. Beurskens, T. Biewer, M. Bigi, K. Crombe, E. de la Luna, P. de Vries, W. Fundamenski, S. Gerasimov, C. Giroud, M. Gryaznevich, N. Hawkes, S. Hotchin, D. Howell, S. Jachmich, V. Kiptily, L. Moreira, V. Parail, S. Pinches, E. Rachlew, and O. Zimmermann, *Physical Review Letters* **98**, 265004 (2007).
- <sup>3</sup>Y. M. Jeon, J. K. Park, S. W. Yoon, W. H. Ko, S. G. Lee, K. D. Lee, G. S. Yun, Y. U. Nam, W. C. Kim, J.-G. Kwak, K. S. Lee, H. K. Kim, and H. L. Yang, *Physical Review Letters* **109**, 035004 (2012).
- <sup>4</sup>Y. Sun, Y. Liang, Y. Q. Liu, S. Gu, X. Yang, W. Guo, T. Shi, M. Jia, L. Wang, B. Lyu, C. Zhou, A. Liu, Q. Zang, H. Liu, N. Chu, H. H. Wang, T. Zhang, J. Qian, L. Xu, K. He, D. Chen, B. Shen, X. Gong, X. Ji, S. Wang, M. Qi, Y. Song, Q. Yuan, Z. Sheng, G. Gao, P. Fu, and B. Wan, *Physical Review Letters* **117**, 115001 (2016).
- <sup>5</sup>W. Suttrop, A. Kirk, R. Nazikian, N. Leuthold, E. Strumberger, M. Willensdorfer, M. Cavedon, M. Dunne, R. Fischer, S. Fietz, J. C. Fuchs, Y. Q. Liu, R. M. McDermott, F. Orain, D. A. Ryan, E. Viezzer, the ASDEX Upgrade Team, The DIII-D Team, and the EUROfusion MST1 Team, *Plasma Physics and Controlled Fusion* **59**, 014049 (2016).
- <sup>6</sup>J. K. Park, Y. Jeon, Y. In, J.-W. Ahn, R. Nazikian, G. Park, J. Kim, H. Lee, W. Ko, H.-S. Kim, N. C. Logan, Z. Wang, E. A. Feibush, J. E. Menard, and M. C. Zarnstropp, *Nature Physics* **14**, 1223 (2018).
- <sup>7</sup>A. B. Rechester and M. N. Rosenbluth, *Physical Review Letters* **40**, 38 (1978).
- <sup>8</sup>G. Park, C. S. Chang, I. Joseph, and R. A. Moyer, *Physics of Plasmas* **17**, 102503 (2010).
- <sup>9</sup>P. B. Snyder, T. H. Osborne, K. H. Burrell, R. J. Groebner, A. W. Leonard, R. Nazikian, D. M. Orlov, O. Schmitz, M. R. Wade, and H. R. Wilson, *Physics of Plasmas* **19**, 056115 (2012).
- <sup>10</sup>R. Nazikian, C. Paz-Soldan, J. D. Callen, J. S. DeGrassie, D. Eldon, T. E. Evans, N. M. Ferraro, B. A. Grierson, R. J. Groebner, S. R. Haskey, C. C. Hegna, J. D. King, N. C. Logan, G. R. McKee, R. A. Moyer, M. Okabayashi, D. M. Orlov, T. H. Osborne, J. K. Park, T. L. Rhodes, M. W. Shafer, P. B. Snyder, W. M. Solomon, E. J. Strait, and M. R. Wade, *Physical Review Letters* **114**, 105002 (2015).
- <sup>11</sup>M. R. Wade, R. Nazikian, J. S. T. E. Evans, N. M. Ferraro, R. A. Moyer, D. M. Orlov, R. J. Buttery, M. E. Fenstermacher, A. M. Garofalo, M. a. Lanctot, G. R. McKee, T. H. Osborne, M. a. Shafer, W. M. Solomon, P. B. Snyder, W. Suttrop, A. Wingen, E. A. Unterberg, and L. Zeng, *Nuclear Fusion* **55**, 023002 (2015).

- <sup>12</sup>Q. M. Hu, R. Nazikian, B. A. Grierson, N. C. Logan, C. Paz-Soldan, and Q. Yu, *Nuclear Fusion* **60**, 076001 (2020).
- <sup>13</sup>G. R. McKee, Z. Yan, C. Holland, R. J. Buttery, T. E. Evans, R. A. Moyer, S. Mordijck, R. Nazikian, T. L. Rhodes, O. Schmitz, and M. R. Wade, *Nuclear Fusion* **53**, 113011 (2013).
- <sup>14</sup>J. Lee, G. S. Yun, M. J. Choi, J.-M. Kwon, Y.-M. Jeon, W. Lee, N. C. Luhmann, and H. K. Park, *Physical Review Letters* **117**, 075001 (2016).
- <sup>15</sup>C. Sung, G. Wang, T. L. Rhodes, S. P. Smith, T. H. Osborne, M. Ono, G. R. McKee, Z. Yan, R. J. Groebner, E. M. Davis, L. Zeng, W. A. Peebles, and T. E. Evans, *Physics of Plasmas* **24**, 112305 (2017).
- <sup>16</sup>M. Leconte and P. H. Diamond, *Physics of Plasmas* **19**, 055903 (2012).
- <sup>17</sup>S. Taimourzadeh, L. Shi, Z. Lin, R. Nazikian, I. Holod, and D. Spong, *Nuclear Fusion* **59**, 046005 (2019).
- <sup>18</sup>F. L. Waelbroeck, J. W. Connor, and H. R. Wilson, *Physical Review Letters* **87**, 215003 (2001).
- <sup>19</sup>Z. X. Wang, J. Q. Li, Y. Kishimoto, and J. Q. Dong, *Physics of Plasmas* **16**, 060703 (2009).
- <sup>20</sup>A. Ishizawa and P. H. Diamond, *Physics of Plasmas* **17**, 074503 (2010).
- <sup>21</sup>M. Sato and A. Ishizawa, *Physics of Plasmas* **24**, 082501 (2017).
- <sup>22</sup>M. J. Choi, L. Bardóczi, J.-M. Kwon, T. S. Hahm, H. K. Park, J. Kim, M. Woo, B.-H. Park, G. S. Yun, E. Yoon, and G. McKee, *Nature Communications* **12**, 375 (2021).
- <sup>23</sup>B. P. van Milligen, E. Sánchez, T. Estrada, C. Hidalgo, B. Brañas, B. Carreras, and L. García, *Physics of Plasmas* **2**, 3017 (1995).
- <sup>24</sup>G. S. Yun, W. Lee, M. J. Choi, J. Lee, M. Kim, J. Leem, Y. Nam, G. H. Choe, H. K. Park, H. Park, D. S. Woo, K. W. Kim, C. W. Domier, N. C. Luhmann, N. Ito, A. Mase, and S. G. Lee, *Review of Scientific Instruments* **85**, 11D820 (2014).
- <sup>25</sup>H. K. Park, M. J. Choi, S. H. Hong, Y. In, Y. M. Jeon, J. S. Ko, W. H. Ko, J. G. Kwak, J. M. Kwon, J. Lee, J. H. Lee, W. Lee, Y. B. Nam, Y. K. Oh, B. H. Park, J. K. Park, Y. S. Park, S. J. Wang, M. Yoo, S. W. Yoon, J. G. Bak, C. S. Chang, W. H. Choe, Y. Chu, J. Chung, N. Eidietis, H. S. Han, S. H. Hahn, H. G. Jhang, J. W. Juhn, J. H. Kim, K. Kim, A. Loarte, H. H. Lee, K. C. Lee, D. Mueller, Y. S. Na, Y. U. Nam, G. Y. Park, K. R. Park, R. A. Pitts, S. A. Sabbagh, G. S. Yun, and the KSTAR team, *Nuclear Fusion* **59**, 112020 (2019).
- <sup>26</sup>O. A. Rosso, H. A. Larrondo, M. T. Martin, A. Plastino, and M. A. Fuentes, *Physical Review Letters* **99**, 154102 (2007).
- <sup>27</sup>P. Beyer, X. Garbet, and P. Ghendrih, *Physics of Plasmas* **5**, 4271 (1998).
- <sup>28</sup>M. Cao and P. H. Diamond, in *Asia-Pacific Transport Working Group* (2021).

- <sup>29</sup>K. C. Lee, J. W. Juhn, Y. U. Nam, Y. S. Kim, H. M. Wi, S. W. Kim, and Y. c. Ghim, *Fusion Engineering and Design* **113**, 87 (2016).
- <sup>30</sup>S. H. Jeong, K. D. Lee, Y. Kogi, K. Kawahata, Y. Nagayama, A. Mase, and M. Kwon, *Review of Scientific Instruments* **81**, 10D922 (2010).
- <sup>31</sup>H. Na, S. Sajjad, J. Park, and M. Kwon, *Fusion Engineering and Design* **86**, 66 (2011).
- <sup>32</sup>G. S. Yun, M. J. Choi, W. Lee, H. K. Park, C. W. Domier, and N. C. Luhmann, *Journal of Instrumentation* **7**, C01024 (2012).
- <sup>33</sup>S. K. Rathgeber, L. Barrera, T. Eich, R. Fischer, B. Nold, W. Suttrop, M. Willensdorfer, E. Wolfrum, and A. U. team, *Plasma Physics and Controlled Fusion* **55**, 025004 (2013).
- <sup>34</sup>Y. C. Kim and E. J. Powers, *IEEE Transactions on Plasma Science* **PS-7**, 120 (1979).
- <sup>35</sup>C. Bandt and B. Pompe, *Physical Review Letters* **88**, 174102 (2002).
- <sup>36</sup>X. Calbet and R. López-Ruiz, *Physical review. E* **63**, 585 (2001).
- <sup>37</sup>M. T. Martin, A. Plastino, and O. A. Rosso, *Physica A: Statistical Mechanics and its Applications* **369**, 439 (2006).
- <sup>38</sup>L. L. Lao, H. S. John, R. D. Stambaugh, A. G. Kellman, and W. Pfeiffer, *Nuclear Fusion* **25**, 1611 (1985).
- <sup>39</sup>S.-K. Kim, R. Shousha, S.-H. Hahn, J. Wai, A. Nelson, S. Yang, J.-K. Park, R. Nazikian, J. Lee, J. Kim, Y.-S. Na, and E. Kolemen, in *The 63rd Annual Meeting of the American Physical Society Division of Plasma Physics* (2021).
- <sup>40</sup>Q. Yu and S. Günter, *Nuclear Fusion* **51**, 073030 (2011).
- <sup>41</sup>C. Paz-Soldan, R. Nazikian, S. R. Haskey, N. C. Logan, E. J. Strait, N. M. Ferraro, J. M. Hanson, J. D. King, M. J. Lanctot, R. A. Moyer, M. Okabayashi, J. K. Park, M. W. Shafer, and B. J. Tobias, *Physical Review Letters* **114**, 105001 (2015).
- <sup>42</sup>J. G. Bak, H. S. Kim, M. K. Bae, J. W. Juhn, D. C. Seo, E. N. Bang, S. B. Shim, K. S. Chung, H. J. Lee, and S. H. Hong, *Journal of Nuclear Materials* **463**, 424 (2015).
- <sup>43</sup>T. Rhee, K. Shinohara, H.-S. Kim, J. M. Kwon, Y. M. Jeon, J. Kim, S.-H. Hahn, J. G. Kwak, S. J. Wang, B. H. Park, and B. Na, *Physics of Plasmas* **26**, 112504 (2019).